Available online at www.sciencedirect.com
ScienceDirect
Trans. Nonferrous Met. Soc. China 22(2012) 2943−2951
Transactions of Nonferrous Metals Society of China
www.tnmsc.cn

Influence of hydrogen content on room temperature compressive properties of Ti−6Al−4V alloy at high strain rate

YUAN Bao-guo[1], YU Hai-ping[2], LI Chun-feng[2]

1. School of Materials Science and Engineering, Hefei University of Technology, Hefei 230009, China;
2. School of Materials Science and Engineering, Harbin Institute of Technology, Harbin 150001, China

Received 29 May 2012; accepted 21 September 2012

Abstract: Electromagnetic forming tests were done at room temperature to reveal the influence of hydrogen content on the compressive properties of Ti−6Al−4V alloy at high strain rate. Microstructure was observed to reveal the mechanism of hydrogen-enhanced compressive properties. The experimental results indicate that hydrogen has favorable effects on the compressive properties of Ti−6Al−4V alloy at high strain rate. Compression of Ti−6Al−4V alloy first increases up to a maximum and then decreases with the increase of hydrogen content at the same discharge energy under EMF tests. The compression increases by 47.0% when 0.2% (mass fraction) hydrogen is introduced into Ti−6Al−4V alloy. The optimal hydrogen content for cold formation of Ti–6Al–4V alloy under EMF was determined. The reasons for the hydrogen-induced compressive properties were discussed.
Key words: Ti−6Al−4V alloy; hydrogen content; electromagnetic forming; compressive property; thermohydrogen processing

1 Introduction

Titanium alloys and magnesium alloys are attractive lightweight structural materials, which have high specific strengths [1−5]. They are widely used in aerospace industry and automobile industry because light weight is being taken seriously by various engineering industries. However, they suffer from low plasticity at room temperature, which restricts their applications [6]. Therefore, how to improve the plasticity of the lightweight materials has been an important research topic.

Recent researches have shown that many methods can significantly enhance the room temperature plasticity of titanium alloys and magnesium alloys, including equal channel angular extrusion (ECAE) [7−9], high pressure torsion (HPT) [10,11], repetitive upsetting-extrusion (RUE) [12,13], accumulative roll-bonding (ARB) [14,15], compound extrusion [16], multi-axial forging (MAF) [17,18], addition of alloying element [19] and thermohydrogen processing (THP) [20,21].

Among the plastification methods of lightweight materials, the thermohydrogen processing is an effective method especially for titanium alloys [22,23]. This is a technique in which hydrogen is used as a temporary alloying element in titanium alloys to control the microstructure and improve the final mechanical properties of titanium alloys. The basis of THP is the modifying effect of hydrogen as an alloying element on phase compositions, development of metastable phases and kinetics of phase transformations in titanium alloys. The addition of hydrogen can refine the microstructure [24,25] and improve the plasticity of titanium alloys at room temperature [26,27] and high temperature [28,29] and superplasticity [30,31]. Among them, the notable characteristic of room temperature hydrogen plastification is the increase of ultimate compression when the first macroscopical crack appears at the cylindrical surface of specimen.

Cold forming is a very economical process for titanium alloy products. But most kinds of titanium alloys are difficult to form at room temperature because of their low plasticity. Although some work has been done on the cold forming of the hydrogenated titanium alloys [26,27], little work has been reported on their compressive properties at high strain rate. Electromagnetic forming (EMF) [32] is an impulse or

Foundation item: Project (51205102) supported by the National Natural Science Foundation of China; Project (2012M511401) supported by the China Postdoctoral Science Foundation; Project (gf201101001) supported by the National Defense Key Disciplines Laboratory of Light Alloy Processing Science and Technology, Nanchang Hangkong University, China
Corresponding author: YUAN Bao-guo; E-mail: yuanbaoguo@163.com
DOI: 10.1016/S1003-6326(11)61554-9

high-speed forming technology, which uses pulsed magnetic fields to apply forces to tubular or sheet metal workpieces, made of a material of high electrical conductivity. EMF has peculiar advantages in forming of metal materials because of the improved formability and strain distribution [33].

Therefore, in this work, EMF tests were carried out at room temperature to reveal the influence of hydrogen content (0.1−0.5%, mass fraction) on the room temperature compressive properties of Ti−6Al−4V alloy at high strain rate. Fracture surface and microstructure were observed to reveal the mechanism of hydrogen-induced compressive properties of Ti−6Al−4V alloy at high strain rate.

2 Experimental

The material used in the present work was a Ti−6Al−4V alloy. Cylindrical specimens, 4 mm in diameter and 6 mm in height, were used for hydrogenation treatment. Details of the hydrogenation process were described in our previous work [34]. The hydrogen contents in the hydrogenated specimens produced in this way were controlled by changing the equilibrium pressure of hydrogen and determined by weighing the specimens before and after hydrogenation using an electronic balance providing a measurement accuracy of 0.01 mg. The specimens with hydrogen contents in the range of 0.1%−0.5% (mass fraction) were obtained.

EMF tests were performed on an EMF 30/5-IV type apparatus at room temperature to investigate the compressive properties of Ti−6Al−4V−*x*H alloys at high strain rate. The parameters of the EMF apparatus are listed in Table 1. Compression was determined by measuring the height of specimens before and after EMF tests, as described by

$$\varepsilon = \frac{H_k - H_0}{H_0} \times 100\% \quad (1)$$

where H_0 is the initial height of specimen before EMF test, H_k is the height of specimen after EMF test, and ε is the compression. The compressive specimens were cylinders of 4 mm in diameter and 6 mm in height. MoS_2 lubricant was coated on the both end faces of the specimen in order to reduce the friction between the specimen and the compressive bars. The specimen was under uniaxial compression instantaneously in EMF test. Capacitance used in EMF test was 2660 μF. The different compressions and ultimate compressions to appearance of the first crack on the lateral surfaces of specimens were obtained by changing the discharge voltage.

Table 1 Parameters of electromagnetic forming apparatus

Machine	Capacitance/ μF	Ceiling voltage/kV	Ceiling energy/ kJ
EMF 30/5-IV	2660	5	33.25

Microstructures were investigated by an optical microscope (Olympus BHM-2UM) and a scanning electron microscope (Hitachi S-570). Fracture surfaces were observed by a scanning electron microscope (Hitachi S-570). Microhardness was determined on a HVS-1000Z digit-display hardness tester with a load of 200 g and a test duration of 15 s.

3 Results and discussion

3.1 EMF tests

The mechanical properties of Ti−6Al−4V−*x*H alloys at different discharge voltages in EMF tests are shown in Table 2. It can be seen that all Ti−6Al−4V−*x*H alloys do not reach their ultimate compressions when the discharge voltage is 0.9 kV, because no crack is found on their lateral surfaces. Compressions of Ti−6Al−4V−*x*H alloys in EMF tests at 0.9 kV are shown in Fig. 1. It can be seen that compression first increases up to a maximum with increasing the hydrogen content and then decreases, which increases by 47.0% when 0.2% hydrogen is introduced into a Ti−6Al−4V alloy. The results indicate that hydrogen has favorable effects on the room temperature compressive deformation of Ti−6Al−4V alloy at high strain rate, which can improve the plasticity of Ti−6Al−4V alloy at room temperature and decrease the demand of forming apparatus and dies.

From Table 2, it can be seen that the compression of specimens with the same hydrogen content increases with the increase of discharge voltage, which is attributed to the increasing discharge energy during the process of EMF tests. Each specimen fractures until it reaches its ultimate compression when the discharge energy reaches one value. However, the discharge energy of the non-hydrogenated specimen is higher than those of the hydrogenated specimens, which indicates that these hydrogenated specimens have lower resistance of deformation and are easier to deform than the non-hydrogenated specimen. Softening of the hydrogenated specimens is mainly attributed to the microstructure evolution after hydrogenation. The amount of softer beta phase and orthorhombic α'' martensites increases after hydrogenation, because hydrogen is a beta-stabilizing element and can decrease the beta transus temperature, as described in our previous work [35].

Table 2 Mechanical properties of Ti−6Al−4V−*x*H alloys at different discharge voltages in EMF tests

Hydrogen content/%	Discharge voltage/ kV	Strain rate/ s^{-1}	Compression/ %	Crack on lateral surface	Does ultimate compression reach?
0.0	0.9	15.4	10.0	no	
0.0	1.0	26.7	17.4	no	
0.0	1.1	39.5	25.7	no	
0.0	1.125	46.6	30.3	no	yes
0.0	1.15	63.2	41.1	yes	
0.0	1.2	67.8	44.1	yes	
0.1	0.9	19.2	12.5	no	
0.1	1.0	29.3	19.0	no	
0.1	1.1	47.7	31.0	no	yes
0.1	1.125	58.7	38.1	yes	
0.1	1.15	71.1	46.2	yes	
0.1	1.2	75.4	49.0	yes	
0.2	0.9	22.7	14.7	no	
0.2	0.95	23.8	15.4	no	
0.2	0.975	29.2	19.0	no	yes
0.2	1.0	50.0	32.5	yes	
0.2	1.1	56.4	36.7	yes	
0.3	0.9	17.7	11.5	no	
0.3	0.925	22.8	14.8	no	yes
0.3	0.95	38.2	24.8	yes	
0.3	1.0	27.2	17.7	yes	
0.3	1.1	62.7	40.8	yes	
0.4	0.9	17.0	11.0	no	
0.4	0.95	18.0	11.7	no	
0.4	0.975	22.1	14.3	no	yes
0.4	1.0	60.4	39.3	yes	
0.4	1.1	−	−	yes	
0.5	0.9	16.8	10.9	no	
0.5	0.95	20.1	13.0	no	
0.5	1.0	31.8	20.7	no	
0.5	1.0	25.0	16.3	no	
0.5	1.025	29.1	19.0	no	yes
0.5	1.05	47.2	30.7	yes	
0.5	1.1	43.6	28.4	yes	

The ultimate compressions of Ti−6Al−4V−*x*H alloys during EMF tests are shown in Fig. 2. It can be seen that the ultimate compression first increases and then decreases with the hydrogen content increasing, which increases by 2.3% when 0.1% hydrogen is introduced into a Ti−6Al−4V alloy, and decreases maximally by 52.7% when the hydrogen content reaches

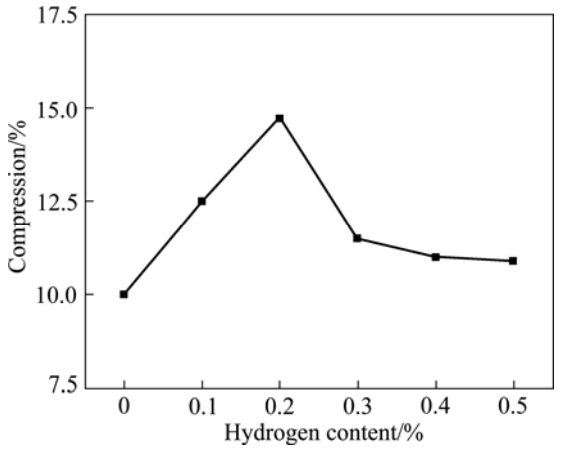

Fig. 1 Compression of Ti−6Al−4V−*x*H alloys in EMF tests at 0.9 kV

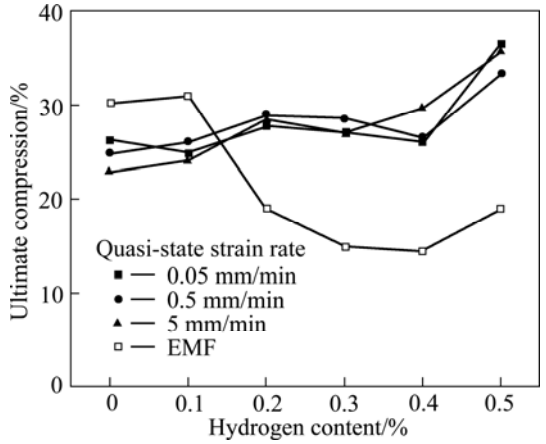

Fig. 2 Ultimate compression of Ti−6Al−4V−*x*H alloys under EMF tests

0.4%. The result indicates that appropriate hydrogen content has a favorable effect on the plasticity of Ti−6Al−4V alloy at high strain rate. And the optimal hydrogen content is 0.1% (mass fraction) for cold deformation of Ti−6Al−4V alloy at high strain rate. However, the optimal hydrogen content for cold deformation of Ti−6Al−4V alloy at high strain rate is lower than that at quasi-state strain rate, and its amplification at high strain rate is smaller than that at quasi-state strain rate. The results of cold deformation of Ti−6Al−4V−*x*H alloys at quasi-state strain rate were described in our previous work [35].

3.2 Fracture surfaces and microstructures after EMF tests

During the process of EMF test, the specimen is under the state of uniaxial compression. The compression of Ti−6Al−4V−*x*H alloy increases with the discharge voltage increasing. When the specimen reaches its ultimate compression, the specimen fails in general into two fragments with the fracture surface at 45° to the

compression axis, which indicates that the shear stress dominates in the process of fracture. Cracks initiate and propagate along the maximum shear stress plane. Fracture surfaces can be observed until these two fragments separate completely. Ti−6Al−4V−0.1H alloy and Ti−6Al−4V−0.4H alloy were selected to observe their fracture surfaces, because the ultimate compression of Ti−6Al−4V−0.1H alloy is the highest and that of Ti−6Al−4V−0.4H alloy is the lowest among these Ti−6Al−4V−*x*H alloys. The fracture surfaces of Ti−6Al−4V−0.1H alloy and Ti−6Al−4V−0.4H alloy after EMF test are shown in Fig. 3. It can be seen that there are two areas on the fracture surfaces of Ti−6Al−4V−*x*H alloys: dimples areas and relative smooth areas, similar to the results of Refs. [36,37]. Commonly, the presence of dimple areas indicates a ductile rupture, which is elongated along the maximum shear stress direction and created under tensile stress within shear band and presents parabolic. While the presence of relative smooth areas implies a brittle rupture, which is believed to be caused by the rubbing of the mating fracture surfaces of specimen while the surfaces were still soft due to the high temperature in the shear band region. There are two differences between the fracture surfaces of Ti−6Al−4V−0.1H alloy and Ti−6Al−4V−0.4H alloy. One difference is that the dimple of Ti−6Al−4V−0.1H alloy is larger than that of Ti−6Al−4V−0.4H alloy. The other is that the area of dimples on the fracture surface of Ti−6Al−4V−0.1H alloy is larger than that of Ti−6Al−4V−0.4H alloy. The results of fracture surfaces in Ti−6Al−4V−*x*H alloys after EMF tests indicate that the plasticity of the specimen with lower hydrogen content is higher than that of the specimen with higher hydrogen content, which is coincident with the ultimate compressions of Ti−6Al−4V−*x*H alloys under EMF tests.

After EMF tests, Ti−6Al−4V−*x*H alloys are cut along their cross sections using an electric discharging machine, polished and etched in a mixed solution of $V(HF):V(HNO_3):V(H_2O)=1:1:8$ to reveal their microstructures. The optical micrographs of Ti−6Al−4V−*x*H alloys are shown in Fig. 4. The white areas in Fig. 4 indicate that the microstructure is homogeneous. Two white adiabatic shear bands (ASBs) are found before each Ti−6Al−4V−*x*H alloy reaches its ultimate compression, in which microvoid and microcrack can be found and no macrocrack is found. These two ASBs

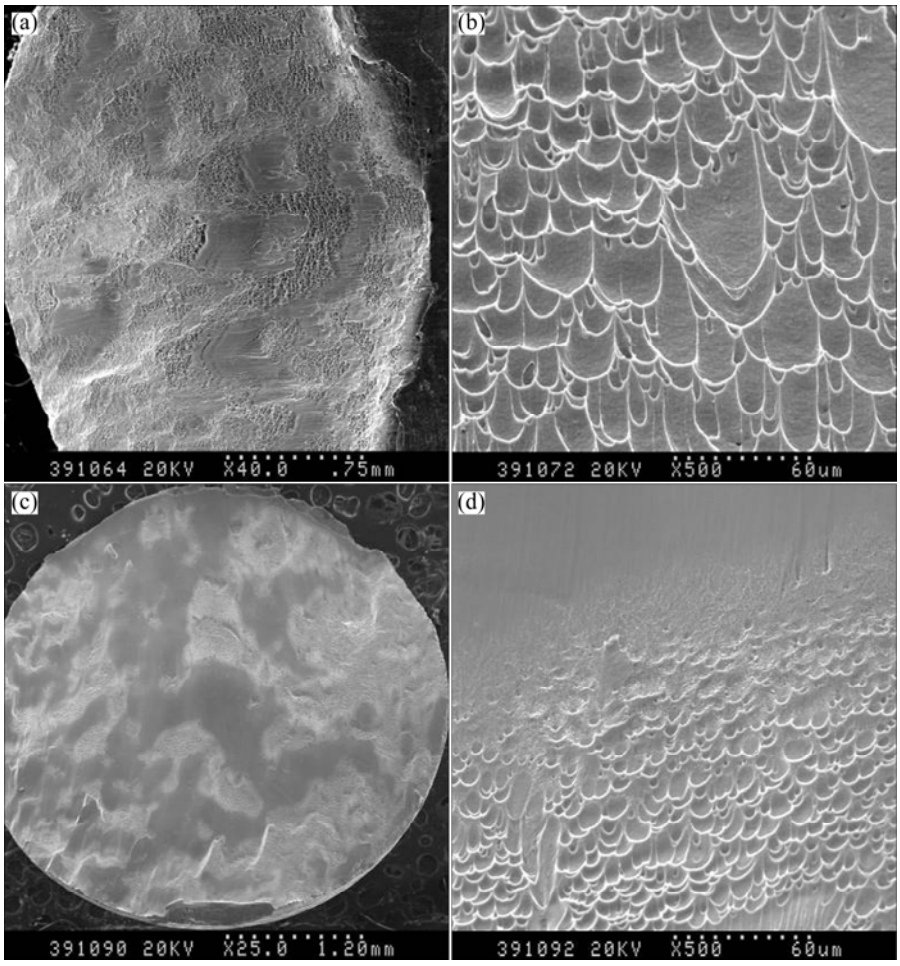

Fig. 3 Fracture surfaces of Ti−6Al−4V−*x*H alloys during EMF test: (a), (b) Ti−6Al−4V−0.1H alloy, 1.15 kV; (c), (d) Ti−6Al−4V−0.4H alloy, 1.0 kV

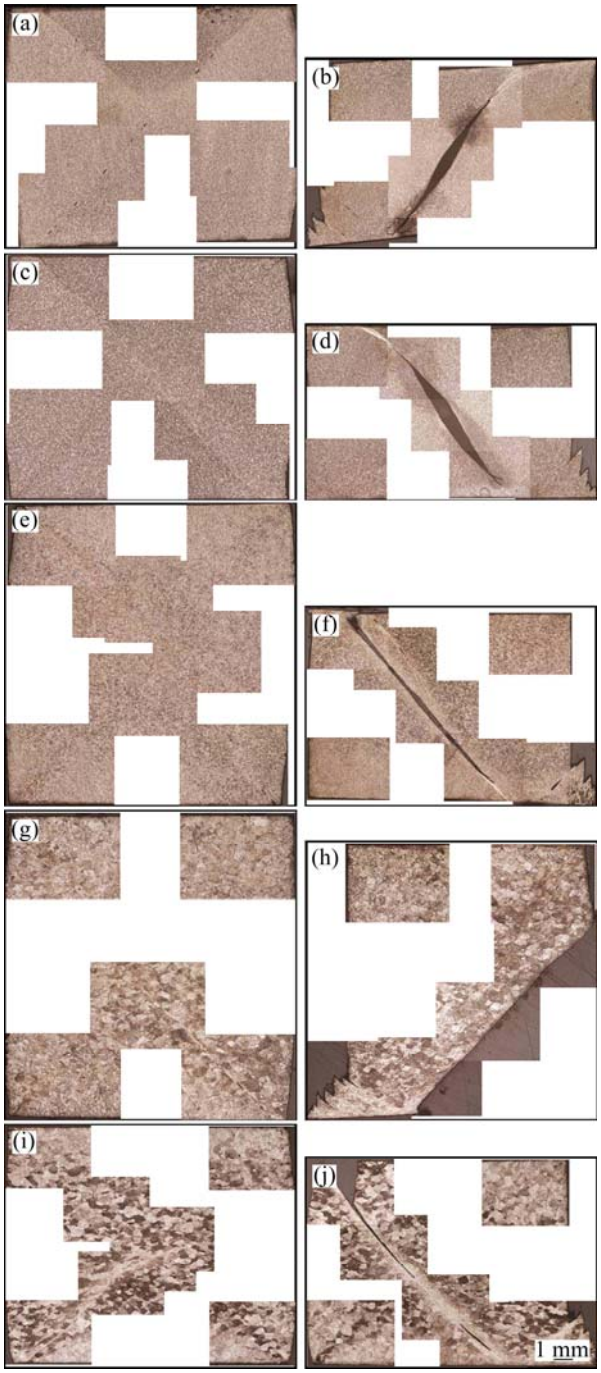

Fig. 4 Optical micrographs of Ti−6Al−4V−*x*H alloys after EMF tests: (a) 0H, 1.125 kV, ultimate compression; (b) Without H, 1.15 kV, after ultimate compression; (c) 0.1%H, 1.1 kV, ultimate compression; (d) 0.1%H, 1.125 kV, after ultimate compression; (e) 0.2%H, 0.975 kV, ultimate compression; (f) 0.2%H, 1.0 kV, after ultimate compression; (g) 0.3%H, 0.925 kV, ultimate compression; (h) 0.3%H, 0.95 kV, after ultimate compression; (i) 0.5%H, 1.025 kV, ultimate compression; (j) 0.5%H, 1.05 kV, after ultimate compression

intersect with each other as 90°. ASBs become more obscure with an increase in the hydrogen content. After Ti−6Al−4V−*x*H alloys reach their ultimate compressions, ASB becomes more obvious. While only one ASB can be found and it intersects with the compression axis as 45°. Macrocrack can be obviously found, and its maximum width decreases from 0.702 mm of the nonhydrogenated Ti−6Al−4V alloy to 0.198 mm of the Ti−6Al−4V−0.5H alloy with the increasing hydrogen content. The results indicate that hydrogen decreases the sensitivity of ASB of Ti−6Al−4V alloy.

More detailed microscopic features of ASBs in Ti−6Al−4V−*x*H alloys are investigated by SEM analysis, which reveals the evolution process of ASB. SEM micrographs of Ti−6Al−4V−*x*H alloys after EMF tests are shown in Fig. 5. It can be seen that there are clear boundaries between ASB and bulk material. Microstructure in ASB is elongated sharply, or even broken. The deformation in ASB is severer than that in bulk material. The characteristic of deformation band can be seen. Vickers hardness in ASB is higher than that in bulk material (as shown in Fig. 6), which is attributed to the strain rate hardening, strain hardening and softening induced by adiabatic temperature rise. The results show that ASB is a deformation band when Ti−6Al−4V−*x*H alloys are deformed under EMF tests.

ASBs in Ti−6Al−4V−*x*H alloys become obscure and the maximum width of macrocrack becomes smaller with the increasing of hydrogen content, which indicates that the sensitivity of ASB in Ti−6Al−4V−*x*H alloys becomes weaker with the increasing of hydrogen content. The appearance of this phenomenon is caused by the increase of thermal conductivity and strain hardening rate in Ti−6Al−4V−*x*H alloys as the hydrogen content increases [36,38]. The reason of the increasing thermal conductivity is that the addition of hydrogen to titanium alloy weakens the atomic bonding, decreases the bonding energy and therefore promotes the transfer of thermal motion. The increase of thermal conductivity leads to the improvement of heat-sinking capability. Strain hardening rate in Ti−6Al−4V−*x*H alloys increases after hydrogenation, as shown in Fig. 7. Therefore, Ti−6Al−4V−*x*H alloys become less sensitive to ASB with the increasing hydrogen content at high strain rate.

The microdamage mode of Ti−6Al−4V−*x*H alloys under EMF is similar and consists of ASB, microvoid and microcrack. Fracture of Ti−6Al−4V−*x*H alloys is prior to create in ASB because ASB is weaker than bulk material due to the presence of microvoid and microcrack in ASB. Wall of microvoid is smooth, which indicates ASB is soft and its temperature in ASB is high [39]. The shape of microvoid presents spheric and ellipsoidal. The long axis of ellipsoidal microvoid is the same as ASB and its width is coincident with the width of ASB, as shown in Fig. 5.

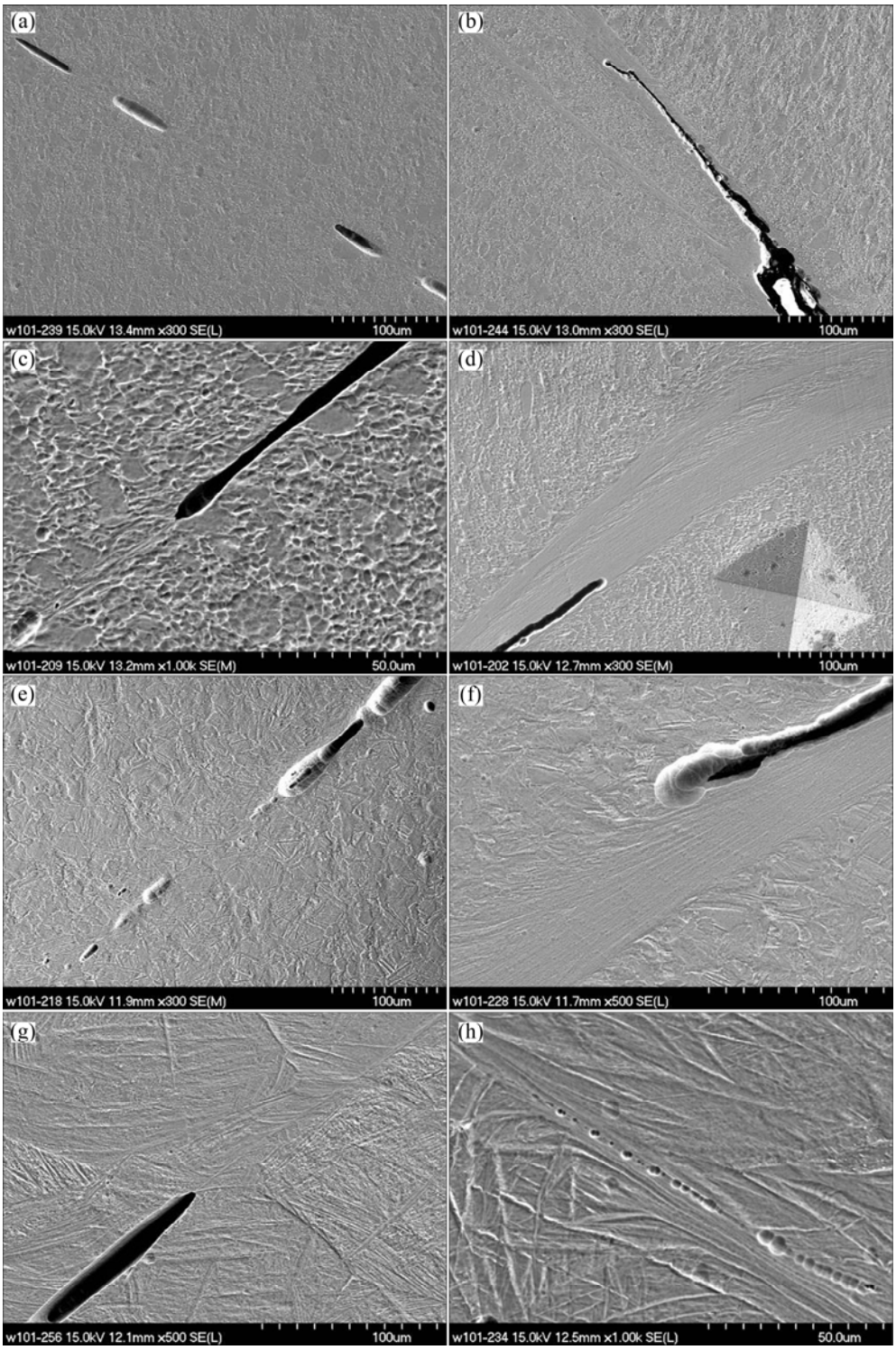

Fig. 5 SEM photos of ASB in Ti−6Al−4V−*x*H alloys: (a) without H, 1.125 kV; (b) without H, 1.15 kV; (c) 0.1%H, 1.1 kV; (d) 0.1%H, 1.125 kV; (e) 0.2%H, 0.975 kV; (f) 0.2%H, 1.0 kV; (g) 0.3%H, 0.925 kV; (h) 0.5%H, 1.025 kV

Fracture of ASB is realized by initiation, growth and connection of microvoids. Microvoid is initiated at high temperature within ASB under tensile stress. The molten microvoid is spheric shape determined by the least-work theory, as shown in Fig. 5(h). With the development of spheric microvoid, it develops along ASB and is hard to develop perpendicular with ASB due to the restriction of bulk material around ASB. Therefore, ellipsoidal microvoid is formed, as shown in Fig. 5(a). Ellipsoidal microvoids grow, connect with each other, and then macrocrack is formed in ASB, which leads to the fracture of specimen along ASB. The shape of microvoid can also be seen at the frontier of crack, as shown in Fig. 5(f).

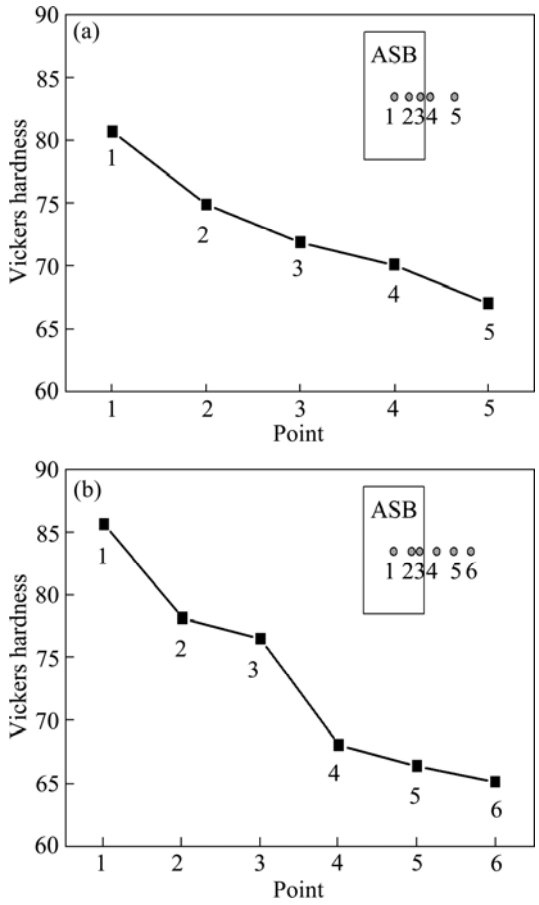

Fig. 6 Vickers hardness of Ti−6Al−4V−*x*H alloys in and out of ASB after EMF tests: (a) Without H, 1.15 kV; (b) 0.1%H, 1.125 kV

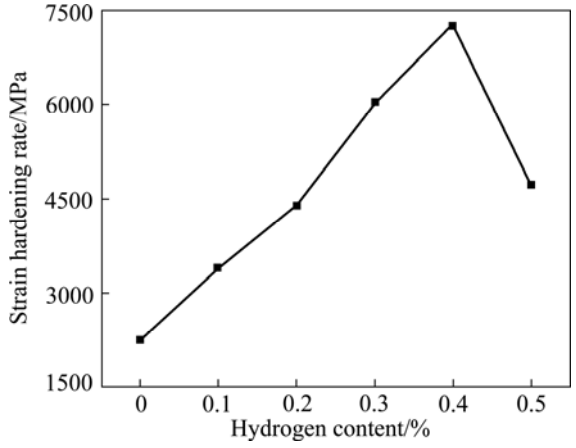

Fig. 7 Strain hardening rate of Ti−6Al−4V−*x*H alloys

4 Conclusions

1) Compression first increases up to a maximum with the hydrogen content increasing and then decreases when Ti−6Al−4V−*x*H alloys are compressed under EMF tests at the same discharge voltage, which indicates that hydrogen can improve the plastic deformation of Ti−6Al−4V alloy at room temperature and decrease the demand of forming apparatus and dies. The compression increases by 47.0% when 0.2% hydrogen is introduced into a Ti−6Al−4V alloy.

2) The compression of specimen charged with the same hydrogen content increases with the increasing of discharge voltage under EMF tests. The ultimate compression first increases up to a maximum with the hydrogen content increasing and then decreases. Its amplification at high strain rate is smaller than that at quasi-state strain rate.

3) ASBs become more obscure and the maximum width of macrocrack decreases with the increase in the hydrogen content, which indicates that the sensitivity of ASB in Ti−6Al−4V−*x*H alloys becomes weaker with the increase of hydrogen content. The appearance of this phenomenon is caused by the increase of thermal conductivity and strain hardening rate in Ti−6Al−4V−*x*H alloys.

References

[1] FUNATANI K. Emerging technology in surface modification of light metals [J]. Surface and Coatings Technology, 2000, 133−134: 264−272.

[2] ZHANG Da-wei, YANG He, SUN Zhi-chao, FAN Xiao-guang. Influences of fillet radius and draft angle on local loading process of titanium alloy T-shaped components [J]. Transactions of Nonferrous Metals Society of China, 2011, 21(12): 2693−2704.

[3] CHEN Jian-chun, PAN Chun-xu. Welding of Ti−6Al−4V alloy using dynamically controlled plasma arc welding process [J]. Transactions of Nonferrous Metals Society of China, 2011, 21(7): 1506−1512.

[4] ZHAO Zu-de, CHEN Qiang, CHAO Hong-ying, HUANG Shu-hai. Microstructural evolution and tensile mechanical properties of thixoforged ZK60-Y magnesium alloys produced by two different routes [J]. Materials & Design, 2010, 31(4): 1906−1916.

[5] ZHAO Zu-de, CHEN Qiang, YANG Lin, SHU Da-yu, ZHAO Zhi-xiang. Microstructure and mechanical properties of Mg−Zn−Y−Zr alloy prepared by solid state recycling [J]. Transactions of Nonferrous Metals Society of China, 2011, 21(2): 265−271.

[6] ZHAO Zu-de, CHEN Qiang, TANG Ze-jun, HU Chuan-kai. Microstructural evolution and tensile mechanical properties of AM60B magnesium alloy prepared by the SIMA route [J]. Journal of Alloys and Compounds, 2010, 497(1−2): 402−411.

[7] ZHAO Zu-de, CHEN Qiang, CHAO Hong-ying, HU Chuan-kai, HUANG Shu-hai. Influence of equal channel angular extrusion processing parameters on the microstructure and mechanical properties of Mg−Al−Y−Zn alloy [J]. Materials & Design, 2011, 32(2): 575−583.

[8] ZHAO Guo-qun, XU Shu-bo, LUAN Yi-guo, GUAN Yan-jin, LUN Ning, REN Xu-fang. Grain refinement mechanism analysis and experimental investigation of equal channel angular pressing for producing pure aluminum ultra-fine grained materials [J]. Materials Science and Engineering A, 2006, 437(2): 281−292.

[9] CHEN Qiang, LUO Shou-jing, ZHAO Zu-de. Microstructural

evolution of previously deformed AZ91D magnesium alloy during partial remelting [J]. Journal of Alloys and Compounds, 2009, 477(1−2): 726−731.

[10] ZHILYAEV A P, LANGDON T G. Using high-pressure torsion for metal processing: Fundamentals and applications [J]. Progress in Materials Science, 2008, 53(6): 893−979.

[11] SERRE P, FIGUEIREDO R B, GAO N, LANGDON T G. Influence of strain rate on the characteristics of a magnesium alloy processed by high-pressure torsion [J]. Materials Science and Engineering A, 2011, 528(10−11): 3601−3608.

[12] CHEN Qiang, ZHAO Zu-de, ZHAO Zhi-xiang, HU Chuan-kai, SHU Da-yu. Microstructure development and thixoextrusion of magnesium alloy prepared by repetitive upsetting-extrusion [J]. Journal of Alloys and Compounds, 2011, 509(26): 7303−7315.

[13] HU Lian-xi, LI Yu-ping, WANG Er-de, YU Yang. Ultrafine grained structure and mechanical properties of a LY12 Al alloy prepared by repetitive upsetting-extrusion [J]. Materials Science and Engineering A, 2006, 422(1−2): 327−332.

[14] PEREZ-PRADO M T, del VALLE J A, RUANO O A. Grain refinement of Mg−Al−Zn alloys via accumulative roll bonding [J]. Scripta Materialia, 2004, 51(11): 1093−1097.

[15] KITAHARA H, UCHIKADO K, MAKINO J, IIDA N, TSUSHIDA M, TSUJI N, ANDO S, TONDA H. Fatigue crack propagation behavior in commercial purity Ti severely deformed by accumulative roll bonding process [J]. Materials Transactions, 2008, 49(1): 64−68.

[16] CHEN Qiang, ZHAO Zhi-xiang, SHU Da-yu, ZHAO Zu-de. Microstructure and mechanical properties of AZ91D magnesium alloy prepared by compound extrusion [J]. Materials Science and Engineering A, 2011, 528(10−11): 3930−3934.

[17] BISWAS S, SUWAS S. Evolution of sub-micron grain size and weak texture in magnesium alloy Mg−3Al−0.4Mn by a modified multi-axial forging process [J]. Scripta Materialia, 2012, 66(2): 89−92.

[18] ZHAO Zu-de, CHEN Qiang, Hu Chuan-kai, Shu Da-yu. Microstructure and mechanical properties of SPD-processed an as-cast AZ91D+Y magnesium alloy by equal channel angular extrusion and multi-axial forging [J]. Materials & Design, 2009, 30(10): 4557−4561.

[19] ZHAO Zu-de, CHEN Qiang, WANG Yan-bin, SHU Da-yu. Microstructures and mechanical properties of AZ91D alloys with Y addition [J]. Materials Science and Engineering A, 2009, 515(1−2): 152−161.

[20] FROES F H, SENKOV O N, QAZI J O. Hydrogen as a temporary alloying element in titanium alloys: Thermohydrogen processing [J]. International Materials Reviews, 2004, 49(3−4): 227−245.

[21] YUAN Bao-guo, LI Chun-feng, YU Hai-ping, SUN Dong-li. Influence of hydrogen content on tensile and compressive properties of Ti−6Al−4V alloy at room temperature [J]. Materials Science and Engineering A, 2010, 527(16−17): 4185−4190.

[22] ELIEZER D, ELIAZ N, SENKOV O N, FROES F H. Positive effects of hydrogen in metals [J]. Materials Science and Engineering A, 2000, 280(1): 220−224.

[23] SENKOV O N, FROES F H. Thermohydrogen processing of titanium alloys [J]. International Journal of Hydrogen Energy, 1999, 24(6): 565−576.

[24] ZHAO Jing-wei, DING Hua, ZHONG Yu-rong, LEE C S. Effect of thermo hydrogen treatment on lattice defects and microstructure refinement of Ti6Al4V alloy [J]. International Journal of Hydrogen Energy, 2010, 35(12): 6448−6454.

[25] NIU Yong, LI Miao-quan. Application of thermohydrogen processing for formation of ultrafine equiaxed grains in near alpha Ti600 alloy [J]. Metallurgical and Materials Transactions A, 2009, 40(12): 3009−3015.

[26] KOLACHEV B A. Reversible hydrogen alloying of titanium-alloys [J]. Metal Science and Heat Treatment, 1993, 35(9−10): 586−591.

[27] MALKOV A V, KOLACHEV B A. Favorable effect of hydrogen on the plasticity of β titanium alloys [J]. Materials Science, 1977, 13(1): 1−4.

[28] CHEN Ye-xin, WAN Xiao-jing, LI Fang, WANG Qing-jiang, LIU Yu-yin. The behavior of hydrogen in high temperature titanium alloy Ti-60 [J]. Materials Science and Engineering A, 2007, 466(1−2): 156−159.

[29] LI Miao-quan, ZHANG Wei-fu. Effect of hydrogenation content on high temperature deformation behavior of Ti−6Al−4V alloy in isothermal compression [J]. International Journal of Hydrogen Energy, 2008, 33(11): 2714−2720.

[30] NECHAEV Y S, IOURTCHENKO D V, HIRSCHBERG J G, VEZIROGLU T N. On the physics of hydrogen plastification and superplasticity of metallic materials and compounds [J]. International Journal of Hydrogen Energy, 2004, 29(13): 1421−1423.

[31] ZHANG Hao, LAM T F, XU Jia-long, WANG Shi-hong. The effect of hydrogen on the strength and superplastic deformation of beta-titanium alloys [J]. Journal of Materials Science, 1996, 31(22): 6105−6111.

[32] PSYK V, RISCH D, KINSEY B L, TEKKAYA A E, KLEINER M. Electromagnetic forming—A review [J]. Journal of Materials Processing Technology, 2011, 211(5): 787−829.

[33] YU Hai-ping, LI Chun-feng. Effects of coil length on tube compression in electromagnetic forming [J]. Transactions of Nonferrous Metals Society of China, 2007, 17(6): 1270−1275.

[34] YUAN Bao-guo, YU Hai-ping, LI Chunfeng, SUN Dong-li. Effect of hydrogen on fracture behavior of Ti−6Al−4V alloy by in-situ tensile test [J]. International Journal of Hydrogen Energy, 2010, 35(4): 1829−1838.

[35] YUAN Bao-guo, LI Chun-feng, YU Hai-ping, SUN Dong-li. Effect of hydrogen content and stress state on room-temperature mechanical properties of Ti−6Al−4V alloy [J]. Transactions of Nonferrous Metals Society of China, 2009, 19: s423−s428.

[36] LIU Xin-qin, TAN Cheng-wen, ZHANG Jing, HU Yang-guang, MA Hong-lei, WANG Fu-chi, CAI Hong-nian. Influence of microstructure and strain rate on adiabatic shearing behavior in Ti−6Al−4V alloys [J]. Materials Science and Engineering A, 2009, 501(1−2): 30−36.

[37] LIAO S C, DUFFY J. Adiabatic shear bands in a Ti−6Al−4V titanium alloy [J]. Journal of the Mechanics and Physics of Solids, 1998, 46(11): 2201−2231.

[38] WANG Hai-ling. FEM simulation of orthogonal cutting of titanium alloy TC4 with hydrogen [D]. Nanjing: Nanjing University of Aeronautics and Astronautics, 2008: 26.

[39] XUE Q, MEYERS M A, NESTERENKO V F. Self-organization of shear bands in titanium and Ti−6Al−4V alloy [J]. Acta Materialia, 2002, 50(3): 575−596.

氢含量对 Ti−6Al−4V 合金室温高速压缩性能的影响

袁宝国[1]，于海平[2]，李春峰[2]

1. 合肥工业大学 材料科学与工程学院，合肥 230009；
2. 哈尔滨工业大学 材料科学与工程学院，哈尔滨 150001

摘　要：利用电磁成形实验研究氢含量对 Ti−6Al−4V 合金室温高速压缩性能的影响，通过微观组织观察揭示氢致压缩性能机理。结果表明，氢对 Ti−6Al−4V 合金的高速压缩性能存在有益的影响。在电磁成形实验放电能量相同的条件下，Ti−6Al−4V 合金的变形率随氢含量的增加呈先增加后降低的趋势。当 Ti−6Al−4V 合金置氢 0.2%(质量分数)时，合金的变形率增加了 47.0%。确定了有利于 Ti−6Al−4V 合金室温电磁成形时的最佳氢含量。分析了氢致压缩性能的机理。

关键词：Ti−6Al−4V 合金；氢含量；电磁成形；压缩性能；热氢处理

(Edited by YUAN Sai-qian)